MOLEKUL
eISSN: 2503-0310

Articles

https://doi.org/10.20884/1.jm.2022.17.1.5606

The Enrichment of Silver Ions in Ag_3PO_4 through the Morphology Changes and Their Photocatalytic Activities

Uyi Sulaeman[1,*], Khusnul Afifah[1], Hartiwi Diastuti[1], Shu Yin[2]

[1]Department of Chemistry, Jenderal Soedirman University, Purwokerto, 53123, Indonesia
[2]Institute of Multidisciplinary Research for Advanced Materials, Tohoku University, Sendai, 980-8577, Japan

*Corresponding author email: sulaeman@unsoed.ac.id

Received December 20, 2020; **Accepted** December 23, 2021; **Available online** March 20, 2022

ABSTRACT. The Ag_3PO_4 photocatalyst has been developed to degrade the organic pollutant due to its highly active responsive under visible light irradiation. The properties of Ag_3PO_4 may depend on design and preparation. Starting materials and co-precipitation conditions would significantly affect the properties of the product. The controlled defect of this photocatalyst may lead to improve catalytic activity. Here, the unique properties of phosphate deficiency in Ag_3PO_4 were created using the starting material of KH_2PO_4 and $AgNO_3$ under a mixed solvent of water and ethanol. $AgNO_3$ solution with the ethanol percentages of 0%, 25%, 50%, 75% and 90% was added to KH_2PO_4 aqueous solution. The photocatalysts were characterized using XRD, DRS, SEM, and XPS. The changes in morphology can be observed from the tetrahedral to the sphere which has smaller particles. The increased atomic ratio of Ag/P and Ag/O suggests that the silver ion enrichment in Ag_3PO_4 has been created. The activity of Ag_3PO_4 for Rhodamine B elimination increased by 4.3 times higher compared to that of the pristine Ag_3PO_4. The enhanced photocatalytic activity might be caused by the smaller particle size and higher silver ion content on the surface of Ag_3PO_4.

Keywords: Ag_3PO_4, defect, divacancy, photocatalyst, silver ion enrichment.

INTRODUCTION

The design of the photocatalyst was developed worldwide to meet the requirements of environmental applications. This material could be used for organic dye oxidation (Ariyanti, Mailot, & Gao, 2018; Wibowo & Sutanto, 2016), organic pollutant degradation (Kusworo et al., 2021), wastewater treatment (Arifan, Nugraheni, Devara, & Lianandya, 2018) and bacteria degradation (Sutanto, Nurhasanah, & Hidayanto, 2015). The greatest challenge of this material is to produce the highly active photocatalyst under visible light irradiation. Therefore, the enormous energy of sunlight could be harnessed with this technology. The modification of N-doped TiO_2 (Hidayanto, Sutanto, Mukholit, Wibowo, & Irwanto, 2017; Pandiangan, Sutanto, & Nurhasanah, 2018; Sutanto et al., 2017), Fe-TiO_2 (Nasralla, Yeganeh, Astuti, Pitticharoenphun, & Šiller, 2018), and defective TiO_2 nano-powder (Ariyanti, Mills, Dong, Yao, & Gao, 2017), have been prepared to fulfil this purpose. However, low activity has occurred using these materials. Therefore, an alternative photocatalyst should be provided.

Recently, Ag_3PO_4 is a highly active photocatalyst. However, the poor stability of this material prompted researchers around the world to make modifications. The modifications of Ag_3PO_4 through composite (Santos et al., 2020), dopant (Lee et al., 2020), defect (Cruz-Filho et al., 2019), and desired morphology (Wei, Wu, & Lin, 2019), has shown a significant effect on photocatalytic activity. Therefore, the preparation is very pivotal to obtain a highly active photocatalyst. The most interesting thing about the modification of Ag_3PO_4 is the morphology control since the properties of the photocatalytic activity are strongly dependent on the morphology of Ag_3PO_4. The morphology of cubic (Yan et al., 2013), a tetrahedron (Dong, P. Wang, S. Wang, Lei, & Y. Wang, 2014), tetrapod (L. Dong et al., 2014; Wang et al., 2012), rhombic dodecahedral (Xie et al., 2016), nanoflake (Xu, Zhang, Xhang, J. Zhu, & R. Zhu, 2020), and porous nanotubes (Wan et al., 2015b) have been successfully designed. The desired morphology can be treated under different solutions and different starting materials.

The preparation using oleic acid can generate the formation of homogeneous tetrahedral morphology (P. Dong et al., 2014). This tetrahedral morphology exhibited enhanced photocatalytic activity compared to the spherical Ag_3PO_4. The different sources of phosphate ion in preparation of Ag_3PO_4 could also produce different morphology, for example, the microcrystal of Ag_3PO_4 tetrahedrons can be prepared using $AgNO_3$ in ethanol and H_3PO_4 that exhibit high activity (Martin, Umezawa, Chen, Ye, & Tang, 2013; Sulaeman, Febiyanto, Yin, & Sato, 2016). The ethanol

in preparation of Ag_3PO_4 has two roles (Zhang et al., 2018). First, the Ag^+ can be complexed with ethanol due to the strong interaction between oxygen and Ag^+ ion that decreases the diffusion rate of Ag^+ cation. Second, the adsorption of ethanol on {111} facets which has a rich Ag^+, can stabilize their high-energy surfaces. The active site plane of {111} has contributed to improving the catalytic activities (Wan et al., 2015). It is because the {111} facets contain only Ag^+ cation (Hu et al., 2013). Tetrahedron Ag_3PO_4 microcrystal with round edges and corners can also be synthesized by adsorption of potassium ion of KH_2PO_4 on {111} facets (L. Dong et al., 2014). These potassium ions can be adsorbed selectively on {111} facets of Ag_3PO_4 and form tetrahedrons at the proper amount. The properties of catalytic activity are also significantly affected by morphology that is adjusted under the elevated concentration of KH_2PO_4 (Afifah, Andreas, Hermawan, & Sulaeman, 2019). It is very challenging to synthesize the desired morphology that has high photocatalytic activity.

Besides morphology, the defect site on Ag_3PO_4 also has a role significant in photocatalytic reactions. Various defects have been observed in Ag_3PO_4 such as oxygen vacancies, silver vacancies, and OH defects. The preparation of Ag_3PO_4 using CH_3COOAg and $AgNO_3$ followed by the calcination generating a metallic silver and oxygen vacancy in Ag_3PO_4 (P. Dong et al., 2016). The calcination is the key role that generates the oxygen vacancy in Ag_3PO_4 (Chong et al., 2016). These oxygen vacancies can create shallow donor states below the CB and enrich the electron, thus enhancing the conductivity and increasing active sites (Amano & Nakata, 2014). Another defect, the Ag vacancies are formed in the synthesis of Ag_3PO_4/GO using the material of Na_2HPO_4 and $AgNO_3$, polyvinyl pyrrolidone, and graphene oxide (Liu et al., 2018). These vacancies can act as trapping centres of photogenerated holes. The photogenerated electrons on the CB (conduction band) may directly transfer to GO (graphene oxide), whereas the photogenerated holes are trapped by the surface of Ag vacancies, which leads to the high efficiency of charge separation. The defects are spontaneously formed on the surface of Ag_3PO_4. However, in some cases, the large defect inhibits photocatalytic activity (Chen et al., 2014). It is because the large defect can be the centre of photogenerated electron and hole recombination. This defect can be suppressed by annealing treatment (Chen et al., 2014). The defect could also have a negative effect such as OH defects found in the Ag_3PO_4 (Zhang, Zhang, & Song, 2014). However, this typical defect can be decreased by a dopant of Bi^{3+} that leads to improving activity. Based on these phenomena, forming, controlling, and handling the defects are very pivotal.

Herein, the design of Ag_3PO_4 through the morphology control can be realized using the starting material of KH_2PO_4 and $AgNO_3$ under variation mixed ethanol-water solution. This preparation method has not been yet reported by other researchers. The changes in morphology from tetrahedral to sphere can significantly be obtained in the synthesis using 75% ethanol. The ethanol and KH_2PO_4 could play a key role in changing the morphology and properties of Ag_3PO_4. The detailed investigation was also carried out using the XPS analysis and found significant differences in spectra and atomic ratio. The atomic ratio of Ag/P and Ag/O increased under preparation in ethanol 75% that indicating the enrichment of Ag^+ in the surface of Ag_3PO_4. This phenomenon was greatly affecting photocatalytic activity.

EXPERIMENTAL SECTION

The materials used in the synthesis were of analytical grade and used as received without further purification. Silver nitrate ($AgNO_3$), potassium dihydrogen phosphate (KH_2PO_4), absolute ethanol (C_2H_5OH), and Rhodamine B (RhB) was purchased from Merck (made in Germany).

The modified Ag_3PO_4 was prepared using the co-precipitation method based on the previous method (Sulaeman, Hermawan, Andreas, Abdullah, & Yin, 2018), with a new modification using KH_2PO_4 as a source of phosphate ion. The starting material of $AgNO_3$ was dissolved in a mixed solvent of ethanol-water with an ethanol percentage of 0%, 25%, 50%, 75%, and 90%. Typically, 1 gram of $AgNO_3$ was dissolved in 50 ml ethanol solution. $AgNO_3$ ethanol solution was slowly added (dropwise) by KH_2PO_4 solution. The KH_2PO_4 was made by dissolving 0.82 grams into 20 ml of water. The precipitates were separated and washed with water and acetone, dried in an oven at 105°C. The samples were named A-0, A-25, A-50, A-75 and A-90, for the ethanol content of 0%, 25%, 50%, 75% and 90%, respectively.

The Ag_3PO_4 samples were characterized by XRD (Shimadzu XRD-7000), using the X-ray Cu (Kα=1.54056 Å, 30 kV, 30 mA) with scan range (2θ) of 10-80 deg, step width of 0.02 deg and a scan speed of 3 deg/min. A DRS (Shimadzu UV–2450) was utilized to measure the absorption spectra of samples with the wavelength range of 370-800 nm. The bandgap energies were calculated using Tauc's relation at direct transition (Gao, Masuda, & Koumoto, 2003). The morphologies were investigated using SEM (Jeol JSM-6510) with the magnification of 3000 times and 10000 times. The chemistry state in the surface was studied using X-ray photoelectron spectroscopy (Perkin Elmer PHI 5600), and the deconvolution of spectra utilized the XPSPEAK 4.1. The photocatalytic activities were examined through a rate of Rhodamine B degradation (RhB solution: 100 mL, 10 mg/L) with 0.1 g of photocatalyst (Sulaeman et al., 2018). The mixture was stirred at room temperature for 20 minutes (dark conditions) and continued with the irradiation of blue light (LED, 2.5 W, λ=445 nm). Four

ml of the solution was withdrawn and separated from the catalyst using centrifugation every 10 minutes. The RhB in the solution was further measured using a spectrophotometer.

RESULTS AND DISCUSSION

The Ag_3PO_4 samples of A-0, A-25, A-50, A-75, and A-90 have been successfully synthesized. All of the products are powder with a yellow colour. To understand their structures and properties, two samples of A-0 and A-75 were investigated as a control ($AgNO_3$ solution) and treated sample (ethanol solution), respectively. **Figure 1** shows the XRD profile of A-0 and A-75. The structure of the body-centred cubic (JCPDS no.06-0505) with the space group of P4-3n was observed in both the A-0 and the A-75. The FWHM of A-75 shows higher than that of A-0 (**Table 1**). The lower intensity of A-75 suggested that this preparation decreased the crystallinity. The {222}/{200} planes intensity ratio of A-75 (1.45) is higher than that of A-0 (1.32), indicating that the atom vacancy might occur in the {200} plane. All different profiles of XRD imply that the ethanol addition might affect the co-precipitation of Ag_3PO_4. In this case, ethanol acts as a less dipolar solvent that can influence the directional growth of crystals that changes the morphology, facet, and crystallinity.

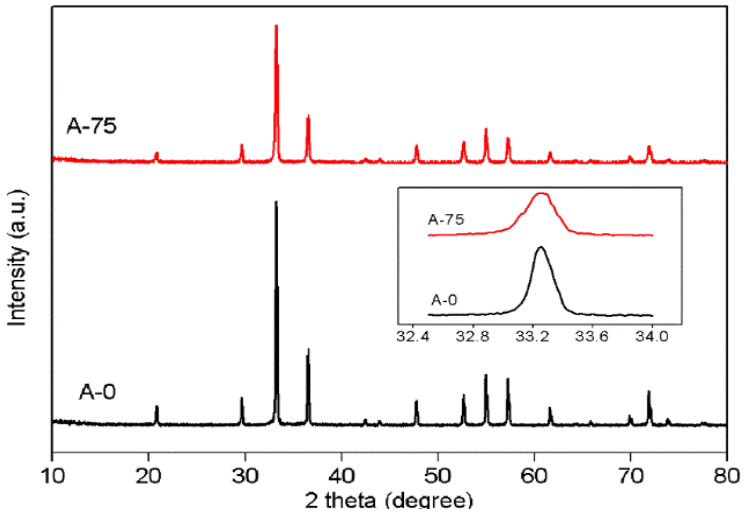

Figure 1. XRD profile of Ag_3PO_4 synthesized using KH_2PO_4 and $AgNO_3$ solution (A-0) and 75% ethanol solution (A-75).

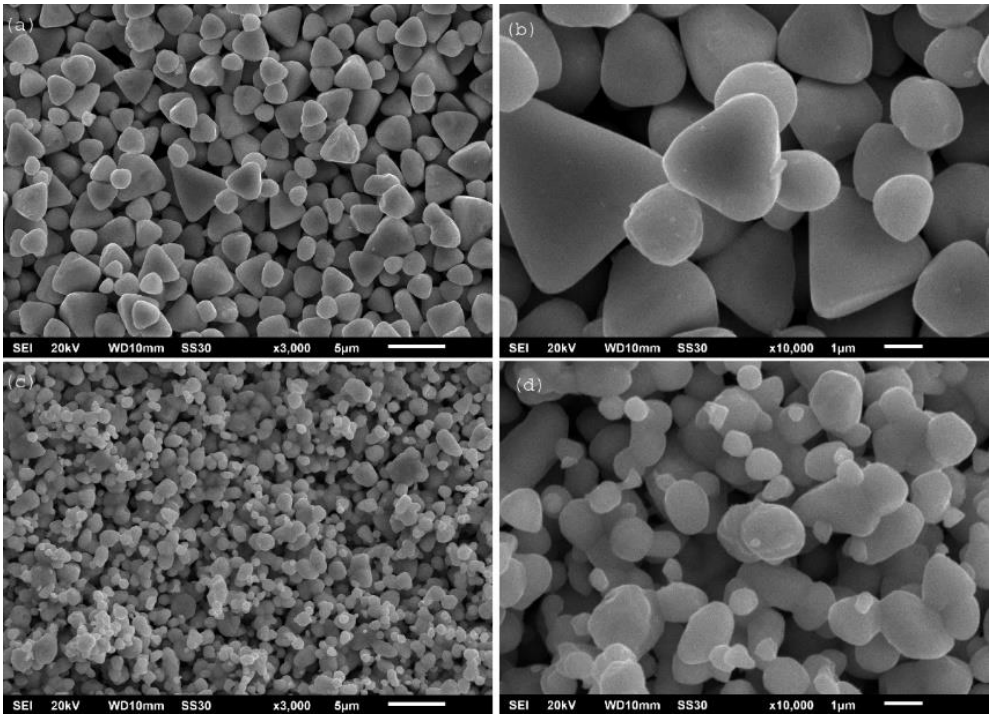

Figure 2. SEM images of Ag_3PO_4 synthesized using KH_2PO_4 and $AgNO_3$ solution (A-0) (**a**) with higher magnification (**b**) and 75% ethanol solution (A-75) (**c**) with higher magnification (**d**).

Table 1. Characteristic of XRD peak at (210) plane

Samples	Peak (degree)	D (Å)	FWHM (degree)	Height (count)
A-0	33.2778	2.69017	0.13700	1380
A-75	33.2616	2.69144	0.22950	727

The morphology of A-0 and A-75 can be seen in **Figure 2**. The morphologies of A-0 were mainly dominated by round edges tetrahedrons with the size of 2-5 µm. This morphology is formed by four triangles of {111} plane (L. Dong et al., 2014; Wan et al., 2015). After adding ethanol in synthesis, the morphologies were dramatically changed into a sphere with particle sizes of 0.5–2 µm. From the SEM images, the utilize of KH_2PO_4 as a phosphate ion source and $AgNO_3$ ethanol solution can significantly affect the sizes and morphologies of Ag_3PO_4. In previous results, the utilize of $Na_2HPO_4.12H_2O$ as source phosphate ion did not produce different morphology between aqueous and mixed ethanol-water solution (Sulaeman et al., 2018), in contrast, when utilizing KH_2PO_4, the changes in morphology were significantly observed, indicating that the potassium ion could be a key factor for tunning the morphology in the system of water-ethanol solution.

Figure 3a showed the optical absorption of A-0 and A-75. The higher absorption intensity of A-0 was observed in both the UV and visible regions. Based on Tauc's relation (**Figure 3b**), the bandgap energy of 2.42 eV and 2.40 was estimated in A-0 and A-75, respectively. The difference of UV-Vis spectra profiles and bandgap energy of A-0 and A-75, suggesting that KH_2PO_4 and ethanol solution significantly affected the co-precipitation of Ag_3PO_4 leading to different optical properties.

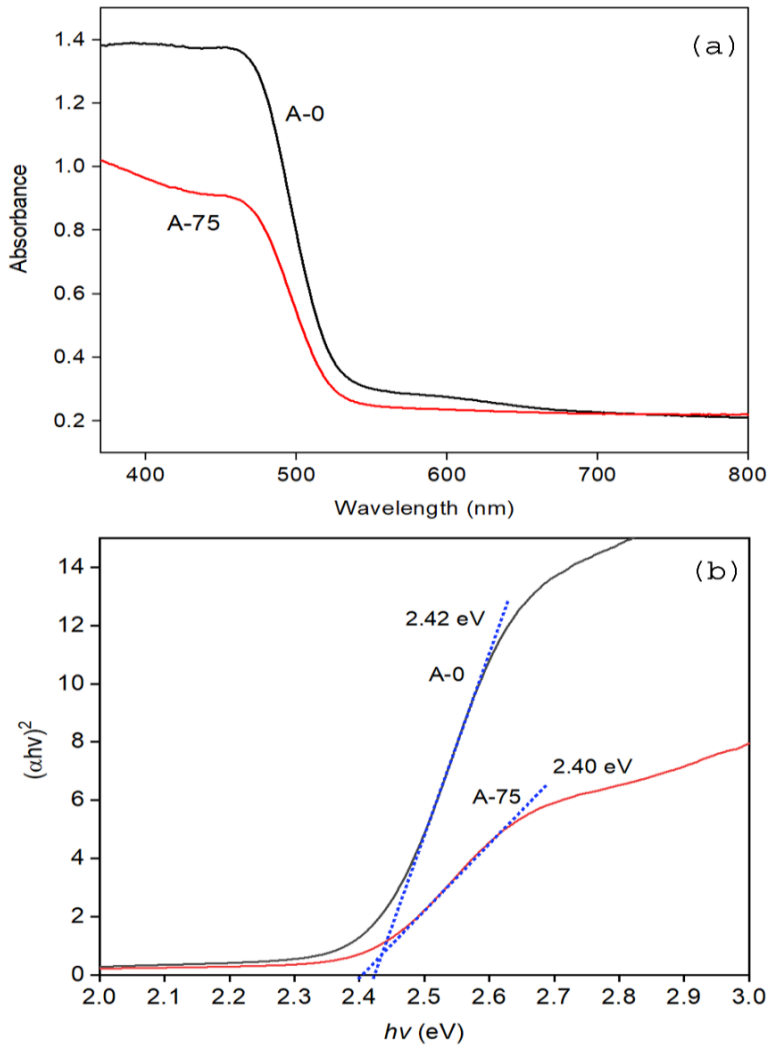

Figure 3. (**a**) DRS of Ag_3PO_4 synthesized using KH_2PO_4 and $AgNO_3$ solution (A-0) and 75% ethanol solution (A-75) and (**b**) the calculation of direct bandgap transition using the plot of hν vs $(\alpha h\nu)^2$

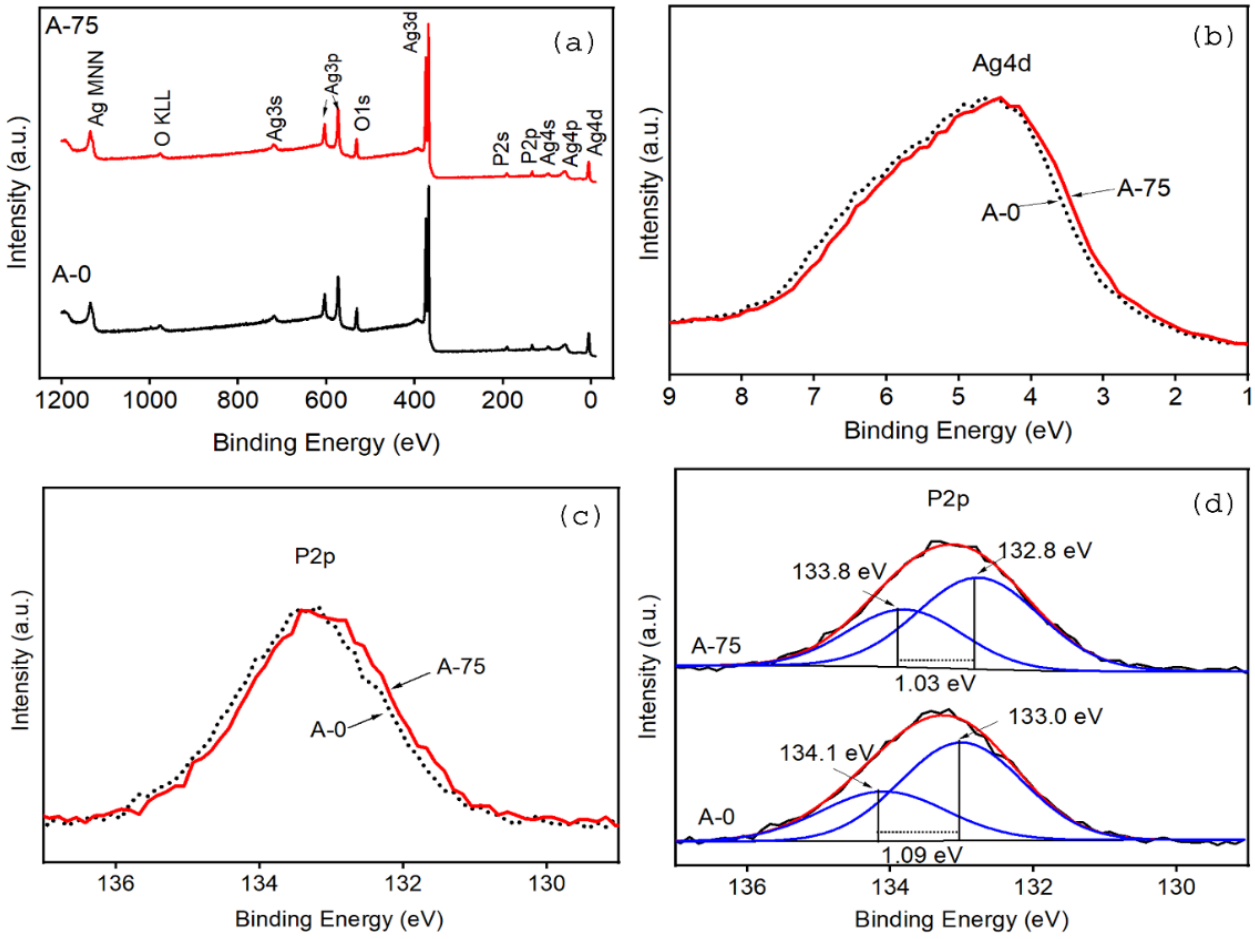

Figure 4. XPS analysis of A-0 and A-75, (**a**) XPS survey, (**b**) spectra of Ag4d, (**c**) P2p, and (**d**) deconvolution of P2p.

Figure 4 displayed the XPS analysis of A-0 and A-75 after Ar^+ sputtering. The elements of Ag, P and O can be observed in the XPS survey (**Figure 4a**). No other elements were significantly found in the samples, indicating the sample was high purity, there are no other compounds chemically bonded on the surface of Ag_3PO_4. There is a shifting of Ag4d and P2p spectra, suggesting that preparation in the ethanol solution affected the chemical state of the samples (**Figure 4b and 4c**). From the deconvolution of P2p, the $P2p_{3/2}$ binding energies of 133.0 eV and 132.8 eV were found in the samples of A-0 and A-75, respectively (Xie et al., 2017), and the $P2p_{1/2}$ binding energy of 134.1 and 133.8 eV were observed in the samples of A-0 and A-75, respectively (**Figure 4d**). It also shows the spin-orbital splitting of 1.09 and 1.03 eV found in the samples of A-0 and A-75, respectively. The lower binding energy and spin-orbital splitting of A-75 implied the changes of interaction between elements. This phenomenon was consistent with DRS analysis that showed the lower bandgap of A-75.

To investigate in detail, the atomic ratios of Ag/P, Ag/O, and O/P were calculated from the XPS data (**Table 2**). The atomic ratio of the sample after and before Ar^+ sputtering is significantly different because they contain many impurities in the surface of Ag_3PO_4 such as water. The atomic ratio of Ag/P and Ag/O after sputtering is higher than that of before sputtering, whereas the ratio of O/P is significantly decreased. Before sputtering, water molecules adsorbed on the surface can increase the oxygen content. After sputtering the oxygen physically adsorbed on the surface was swept out leaving a decrease of oxygen in the surface.

The Ag/P and Ag/O atomic ratio of A-75 is higher than that of A-0, indicating that a small quantity of phosphor and oxygen atom was missing from the samples, resulting in a defect in the surface. The enrichment of silver ions occurred in the A-75. The increased Ag/P and Ag/O atomic ratio of A-75 consistently were found both before and after Ar^+ sputtering. Usually, the high content of Ag^+ ions are found in {111} tetrahedron, but in this result, the high content of Ag^+ is found in the sphere particle, indicating that the high Ag^+ might induce a defect in the lattice of Ag_3PO_4. In other words, the high Ag^+ did not represent the tetrahedron plane. It has already been found that Ag^+ was complexed with ethanol due to strong interaction with the oxygen (Zhang et al., 2018) leading to a coprecipitation of enriched Ag^+ samples.

Table 2. The atomic ratio of P/Ag, O/Ag, and O/P calculated from the XPS analysis

Samples	Before Ar^+ sputtering			After Ar^+ sputtering		
	Ag/P	Ag/O	O/P	Ag/P	Ag/O	O/P
A-0	2.18	0.54	4.04	2.88	0.92	3.11
A-75	2.34	0.58	4.01	2.97	0.95	3.12

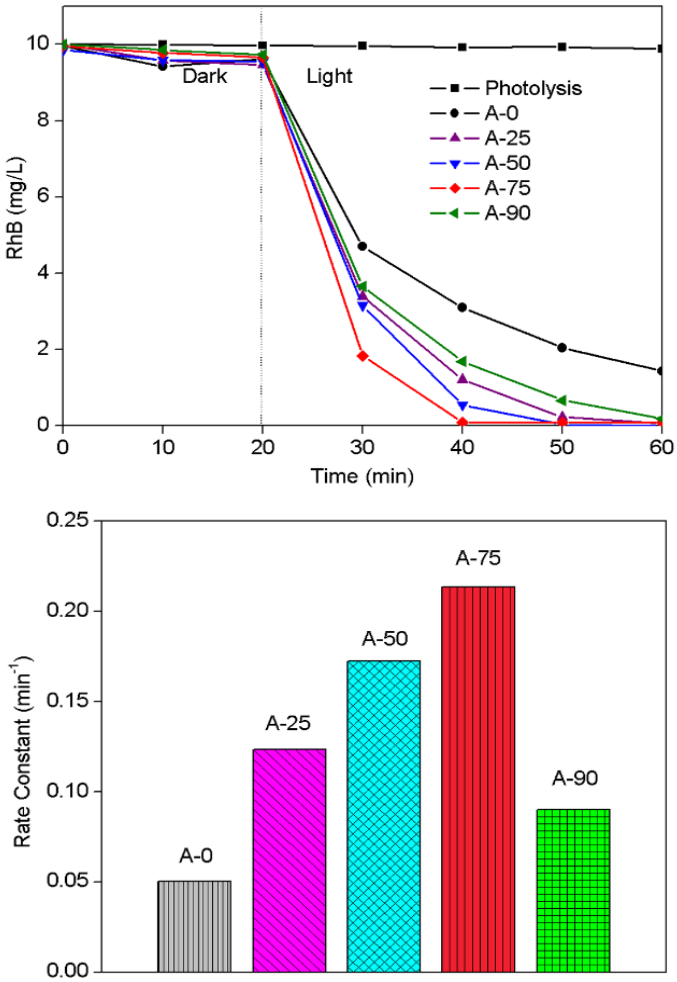

Figure 5. Photocatalytic activity of Ag_3PO_4 synthesized using KH_2PO_4 and $AgNO_3$ solution (A-0) and 75% ethanol solution (A-0, A-25, A-50, A-75, A-90).

The enrichment of silver in Ag_3PO_4 would have three possibilities of defects. The first is the exceed silver ion interstitially incorporated on the lattice of Ag_3PO_4, the second is the formation of phosphate (PO_4^{3-}) vacancy (bulk vacancies), and the third is divacancy of phosphor and oxygen formation. The interstitial silver formation in Ag_3PO_4 is very difficult due to the high ionic radius of silver, it would lead to high strength in the lattice. It is also reported that the silver interstitial favours the tetrahedral site that was coordinated by four O atoms. This phenomenon can act as a shallow donor located above the CBM (conduction band minimum), and stable only in 1+ charge (Reunchan & Umezawa, 2013). Another possibility is the phosphate vacancy, however it is not possible because the data were not supported by XPS results. Phosphate vacancy can be formed when one phosphor atom is missing accompanied by four oxygen atoms (1:4). This phosphate vacancy would result in void formation.

The high possibility of this structure might be a divacancy of phosphorus and oxygen because it matches with the XPS data and the neutrality principle. The phosphor and oxygen are missing together when co-precipitation under ethanol solution. By this proposed argument, the surface formula can be derived from the XPS after Ar^+ sputtering of $Ag_{2.88}PO_{3.11}$ and $Ag_{2.88}P_{0.97}O_{3.03}$ for A-0 and A-75, respectively. The 0.03 mol atomic loss of phosphorus was accompanied by 0.08 mol atomic loss of oxygen (~1:3). Therefore, the enrichment of Ag_3PO_4 might be originated from the divacancy of phosphor and oxygen atoms.

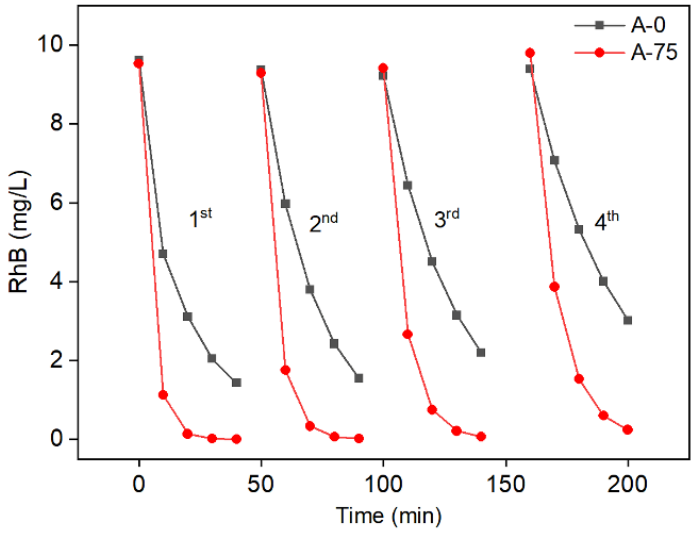

Figure 6. The cycling runs for RhB degradation using Ag_3PO_4 synthesized with KH_2PO_4 and $AgNO_3$ in water (A-0) and ethanol solution (A-75).

The photocatalytic activities of samples were evaluated under blue light irradiation (**Figure 5**). The adsorption in the dark condition for 20 minutes was evaluated. The decrease of RhB due to adsorption is very small, it is 3.4%, 5.4%, 3.1%, 3.0%, and 2.7% for A-0, A-25, A-50, A-75, A-90, respectively. The sample of A-25 exhibits the highest adsorption. Since the highest activity was found in the sample of A-75, suggesting that the adsorption phenomenon might not be the main factor of high catalytic activity.

The rate constants of photocatalytic were determined using the pseudo-first-order kinetic model: $-\ln(C/C_0)=kt$, where C is the RhB concentration at irradiation time t, C_0 is the initial concentration of RhB (Astuti et al., 2017; Wan, Liu, et al., 2015). The rate constant of 0.050, 0.123, 0.172, 0.214 and 0.090 min^{-1} were calculated for A-0, A-25, A-50, A-75 and A-90 respectively. The elevated concentration of ethanol in solution increased the photocatalytic activity of the samples, and the highest catalytic could be observed in A-75, it was 4.3 times higher compared to the A-0. The high photocatalytic activity might be caused by the smaller particle size and enriched Ag^+ surface of Ag_3PO_4 that led to a defect in the surface such as divacancy of phosphorus and oxygen. This defect decreases the bandgap energy and enhances the excitation of electrons from the VB to the CB. The formation of defects might be induced by higher Ag^+ in the surface when the transformation of morphology occurs from the tetrahedron to the sphere. These surface defects can influence the efficiency of e−/h+ separation and suppress the recombination that leads to enhanced photocatalytic activity.

The RhB compound was degraded into the final product of CO_2, H_2O, NO_3^-, NH_4^+, and Cl^- (Sui, Liu, Jiang, & Guo, 2018). The intermediate compounds such as organic acids (carboxyl group) might be formed during photodegradation (Chen, Xiao, Wang, & Ye, 2019), however, due to silver phosphate having strong oxidation, these compounds can no longer exist.

The stabilities of photocatalyst are also evaluated up to four cycles reaction (**Figure 6**). The photocatalyst has remained active for up to four cycles. It is also found that the A-75 exhibits higher activity in every cycle reaction. The activity slightly decreased due to photo corrosion of silver ion in the surface of Ag_3PO_4 forming a metallic silver. This silver metal covered the surface of Ag_3PO_4 and prevented oxidation by blocking incident light (Martin & Umezawa 2013).

CONCLUSIONS

The highly active silver phosphate photocatalyst can be generated by morphology control using $AgNO_3$ and KH_2PO_4 ethanol solution. The KH_2PO_4 as a source of phosphate ion leads to a tetrahedron shape of Ag_3PO_4 under an aqueous solution. Ethanol solution treatment changed the morphology of Ag_3PO_4 into a spherical with smaller particle size and higher Ag^+ content. The enriched Ag^+ in the surface of Ag_3PO_4 might be originated from a divacancy of phosphor and oxygen. These properties significantly enhanced photocatalytic activity.

ACKNOWLEDGMENTS

This research was supported by the Directorate of Research and Community Service, Deputy of Strengthening Research and Development, Ministry of Research and Technology/National Research and Innovation Agency, Number: 176/SP2H/ADM/LT/DRPM/2020.

REFERENCES

Afifah, K., Andreas, R., Hermawan, D., & Sulaeman, U. (2019). Tuning the morphology of Ag_3PO_4 photocatalysts with an elevated concentration of

KH_2PO_4. *Bulletin of Chemical Reaction Engineering & Catalysis*, *14*(3), 625–633.

Amano, F., & Nakata, M. (2014). High-temperature calcination and hydrogen reduction of rutile TiO_2: A method to improve the photocatalytic activity for water oxidation. *Applied Catalysis B: Environmental*, *158–159*, 202–208.

Arifan, F., Nugraheni, F. S., Devara, H. R., & Lianandya, N. E. (2018). Wastewater treatment from Batik Industries using TiO_2 nanoparticles. *IOP Conference Series: Earth and Environmental Science*, *116*, 012046.

Ariyanti, D., Maillot, M., & Gao, W. (2018). Photo-assisted degradation of dyes in a binary system using TiO_2 under simulated solar radiation. *Journal of Environmental Chemical Engineering*, *6*(1), 539–548.

Ariyanti, D., Mills, L., Dong, J., Yao, Y., & Gao, W. (2017). $NaBH_4$ modified TiO_2: Defect site enhancement related to its photocatalytic activity. *Materials Chemistry and Physics*, *199*, 571–576.

Astuti, Y., Arnelli, Pardoyo, Fauziyah, A., Nurhayati, S., Wulansari, A. D., Andianingrum, R., Widiyandari, H., & Bhaduri, G. A. (2017). Studying impact of different precipitating agents on crystal structure, morphology, and photocatalytic activity of bismuth oxide. *Bulletin of Chemical Reaction Engineering & Catalysis*, *12*(3), 478–484.

Chen, D., Wang, Z., Ren, T., Ding, H., Yao, W., Zong, R., & Zhu, Y. (2014). Influence of defects on the photocatalytic activity of ZnO. *Journal of Physical Chemistry C*, *118*(28), 15300–15307.

Chen, J., Xiao, X., Wang, Y., & Ye, Z. (2019). Ag nanoparticles decorated WO_3/g-C_3N_4 2D/2D heterostructure with enhanced photocatalytic activity for organic pollutants degradation. *Applied Surface Science*, *467–468*, 1000–1010.

Chong, R., Cheng, X., Wang, B., Li, D., Chang, Z., & Zhang, L. (2016). Enhanced photocatalytic activity of Ag_3PO_4 for oxygen evolution and Methylene blue degeneration: Effect of calcination temperature. *International Journal of Hydrogen Energy*, *41*(4), 2575–2582.

Cruz-Filho, J. F., Costa, T. M. S., Lima, M. S., Silva, L. J., Santos, R. S., Cavalcante, L. S., Longo, E., & Luz, G. E. (2019). Effect of different synthesis methods on the morphology, optical behavior, and superior photocatalytic performances of Ag_3PO_4 sub-microcrystals using white-light-emitting diodes. *Journal of Photochemistry and Photobiology A: Chemistry*, *377*, 14–25.

Dong, L., Wang, P., Wang, S., Lei, P., & Wang, Y. (2014). A simple way for Ag_3PO_4 tetrahedron and tetrapod microcrystals with high visible-light-responsive activity. *Materials Letters*, *134*, 158–161.

Dong, P., Hou, G., Liu, C., Zhang, X., Tian, H., Xu, F., Xi, X., & Shao, R. (2016). Origin of activity and stability enhancement for Ag_3PO_4 photocatalyst after calcination. *Materials*, *9*(12), 968.

Dong, P., Yin, Y., Xu, N., Guan, R., Hou, G., & Wang, Y. (2014). Facile synthesis of tetrahedral Ag_3PO_4 mesocrystals and its enhanced photocatalytic activity. *Materials Research Bulletin*, *60*, 682–689.

Gao, Y., Masuda, Y., & Koumoto, K. (2003). Band gap energy of $SrTiO_3$ thin film prepared by the liquid phase deposition method. *Journal of the Korean Ceramic Society*, *40*(3), 213–218.

Hidayanto, E., Sutanto, H., Mukholit, Wibowo, S., & Irwanto, M. (2017). Morphology and degradation kinetics of N-doped TiO_2 nano particle synthesized using sonochemical method. *Solid State Phenomena*, *266*, 95–100.

Hu, H., Jiao, Z., Yu, H., Lu, G., Ye, J., & Bi, Y. (2013). Facile synthesis of tetrahedral Ag_3PO_4 submicro-crystals with enhanced photocatalytic properties. *Journal of Materials Chemistry A*, *1*, 2387–2390.

Kusworo, T. D., Susanto, H., Aryanti, N., Rokhati, N., Widiasa, I. N., Al-Aziz, H., Utomo, D. P., Masithoh, D., & Kumoro, A. C. (2021). Preparation and characterization of photocatalytic PSf-TiO_2/GO nanohybrid membrane for the degradation of organic contaminants in natural rubber wastewater. *Journal of Environmental Chemical Engineering*, *9*(2), 105066.

Lee, Y. J., Kang, J. K., Park, S. J., Lee, C. G., Moon, J. K., & Alvarez, P. J. J. (2020). Photocatalytic degradation of neonicotinoid insecticides using sulfate-doped Ag_3PO_4 with enhanced visible light activity. *Chemical Engineering Journal*, *402*, 126183.

Liu, R., Li, H., Duan, L., Shen, H., Zhang, Q., & Zhao, X. (2018). The synergistic effect of graphene oxide and silver vacancy in Ag_3PO_4-based photocatalysts for rhodamine B degradation under visible light. *Applied Surface Science*, *462*, 263–269.

Martin, D. J., Umezawa, N., Chen, X., Ye, J., & Tang, J. (2013). Facet engineered Ag_3PO_4 for efficient water photooxidation. *Energy and Environmental Science*, *6*, 3380–3386.

Nasralla, N. H. S., Yeganeh, M., Astuti, Y., Piticharoenphun, S., & Šiller, L. (2018). Systematic study of electronic properties of Fe-doped TiO_2 nanoparticles by X-ray photoemission spectroscopy. *Journal of Materials Science: Materials in Electronics*, *29*, 17956–17966.

Pandiangan, I. F. D., Sutanto, H., & Nurhasanah, I. (2018). Effect of annealing temperature on optical properties and photocatalytic properties of TiO_2:N 8% thin film for rhodamine B

degradation. *Materials Research Express*, *5*(8), 086404.

Reunchan, P., & Umezawa, N. (2013). Native defects and hydrogen impurities in Ag_3PO_4. *Physical Review B*, *87*, 245205.

Santos, R. K., Martins, T. A., Silva, G. N., Conceição, M. V. S., Nogueira, I. C., Longo, E., & Botelho, G. (2020). Ag_3PO_4/NiO composites with enhanced photocatalytic activity under visible light. *ACS Omega*, *5*(34), 21651–21661.

Sui, Y., Liu, Q., Jiang, T., & Guo, Y. (2018). Synthesis of nano-TiO_2 photocatalysts with tunable Fe doping concentration from Ti-bearing tailings. *Applied Surface Science*, *428*, 1149–1158.

Sulaeman, U., Febiyanto, F., Yin, S., & Sato, T. (2016). The highly active saddle-like Ag_3PO_4 photocatalyst under visible light irradiation. *Catalysis Communications*, *85*, 22–25.

Sulaeman, U., Hermawan, D., Andreas, R., Abdullah, A. Z. A. Z., & Yin, S. (2018). Native defects in silver orthophosphate and their effects on photocatalytic activity under visible light irradiation. *Applied Surface Science*, *428*, 1029–1035.

Sutanto, H., Hidayanto, E., Mukholit, Wibowo, S., Nurhasanah, I., & Hadiyanto. (2017). The physical and photocatalytic properties of N-doped TiO_2 polycrystalline synthesized by a single step sonochemical method at room temperature. *Materials Science Forum*, *890*, 121–126.

Sutanto, H., Nurhasanah, I., & Hidayanto, E. (2015). Deposition of Ag 2~6 mol%-doped ZnO photocatalyst thin films by thermal spray coating method for *E.coli* Bacteria degradation. *Materials Science Forum*, *827*, 3–6.

Wan, J., Liu, E., Fan, J., Hu, X., Sun, L., Tang, C., Yin, Y., Li, H., & Hu, Y. (2015a). In-situ synthesis of plasmonic Ag/Ag_3PO_4 tetrahedron with exposed {111} facets for high visible-light photocatalytic activity and stability. *Ceramics International*, 41, 6933–6940.

Wan, J., Sun, L., Fan, J., Liu, E., Hu, X., Tang, C., & Yin, Y. (2015b). Facile synthesis of porous Ag_3PO_4 nanotubes for enhanced photocatalytic activity under visible light. *Applied Surface Science*, *355*, 615–622.

Wang, H., He, L., Wang, L., Hu, P., Guo, L., Han, X., & Li, J. (2012). Facile synthesis of Ag_3PO_4 tetrapod microcrystals with an increased percentage of exposed {110} facets and highly efficient photocatalytic properties. *CrystEngComm*, *14*, 8342–8344.

Wei, T. T., Wu, T., & Lin, Y. W. (2019). Controlled synthesis of Ag_3PO_4 microparticles with different morphologies and their photocatalytic degradation of rhodamine B under white light-emitting diode irradiation. *Micro & Nano Letters*, *14*, 363–366.

Wibowo, S., & Sutanto, H. (2016). Preparation and characterization of double layer thin films ZnO/ZnO:Ag for methylene blue photodegradation. *AIP Conference Proceedings*, *1710*, 030049.

Xie, Q., Li, Y., Lv, Z., Zhou, H., Yang, X., Chen, J., & Guo, H. (2017). Effective adsorption and removal of phosphate from aqueous solutions and eutrophic water by Fe-based MOFs of MIL-101. *Scientific Reports*, *7*, 3316.

Xie, Y., Huang, Z., Zhang, Z., Zhang, X., Wen, R., Liu, Y., Fang, M., & Wu, X. (2016). Controlled synthesis and photocatalytic properties of rhombic dodecahedral Ag_3PO_4 with high surface energy. *Applied Surface Science*, *389*, 56–66.

Xu, Y., Zhang, X., Zhang, Y., Zhu, J., & Zhu, R. (2020). Nano flake Ag_3PO_4 enhanced photocatalytic activity of bisphenol A under visible light irradiation. *Colloids and Interface Science Communications*, 37, 100277.

Yan, X., Gao, Q., Qin, J., Yang, X., Li, Y., & Tang, H. (2013). Morphology-controlled synthesis of Ag_3PO_4 microcubes with enhanced visible-light-driven photocatalytic activity. *Ceramics International*, *39*, 9715–9720.

Zhang, G. Y., Wei, X. M., Bai, X., Liu, C. M., Wang, B. Y., & Liu, J. W. (2018). Ethanol-water ambient precipitation of {111} facets exposed Ag_3PO_4 tetrahedra and its hybrid with graphene oxide for outstanding photoactivity and stability. *Inorganic Chemistry Frontiers*, *5*, 951–961.

Zhang, S. S., Zhang, S. S., & Song, L. (2014). Super-high activity of Bi^{3+} doped Ag_3PO_4 and enhanced photocatalytic mechanism. *Applied Catalysis B: Environmental*, *152–153*, 129–139.